Journal of Quantitative Spectroscopy & Radiative Transfer 210 (2018) 111–115

Contents lists available at ScienceDirect

Journal of Quantitative Spectroscopy & Radiative Transfer

journal homepage: www.elsevier.com/locate/jqsrt

Frequency metrology of the acetylene lines near 789 nm from lamb-dip measurements

Lei-Gang Tao[a], Tian-Peng Hua[a], Yu R. Sun[a,b], Jin Wang[a], An-Wen Liu[a,b], Shui-Ming Hu[a,b,*]

[a] Hefei National Laboratory for Physical Sciences at Microscale, iChem center, University of Science and Technology of China, Hefei 230026, China
[b] CAS Center for Excellence in Quantum Information and Quantum Physics, University of Science and Technology of China, Hefei 230026, China

ARTICLE INFO

Article history:
Received 4 December 2017
Revised 13 February 2018
Accepted 13 February 2018
Available online 14 February 2018

Keywords:
Cavity ring-down spectroscopy
Acetylene
Frequency metrology
Lamb dip

ABSTRACT

Lamb-dips of the ro-vibrational lines of $^{12}C_2H_2$ near 789 nm were recorded using cavity ring-down saturation spectroscopy. Calibrated by an optical frequency comb, frequencies of 45 acetylene lines were determined with an accuracy of 1.1×10^{-7} cm^{-1} ($\delta\nu/\nu = 8 \times 10^{-12}$), which is over two orders of magnitude more accurate than previous Doppler-limited studies. An averaged shift of about 0.01 cm^{-1} were found by comparing the upper energies obtained in this work to those recently presented by Chubb et al. from a MARVEL analysis.

1. Introduction

The tetratomic linear molecule acetylene is in the focus of various studies of chemical dynamics [1], organic chemistry [2], and industrial chemistry [3]. The spectra of acetylene spread from the infrared to the ultraviolet, and have been used to detect its presence in atmospheres of planets [4], stars [5], and in the interstellar medium [6]. A review of the ro-vibrational spectroscopy of C_2H_2 in the $\tilde{X}^1\Sigma_g^+$ electronic ground state [7] was given by Amyay et al. Lyulin and Prevalov recently presented [8] a data bank of the high-resolution and high-temperature acetylene lines below 10,000 cm^{-1}. Based on the measured high-resolution spectra, Chubb et al. derived more than eleven thousand energy levels of $^{12}C_2H_2$ in the electronic ground state using the MARVEL (measured active rotational-vibrational energy levels) method [9]. Strong acetylene lines in the near infrared can be easily saturated by continuous-wave lasers, and their Lamb-dips have been often used to stabilize laser frequencies [10,11]. Saturation spectra of the C_2H_2 lines near 1.54 μm, belonging to the $\nu_1 + \nu_3$ band, have been extensively studied [12–17]. Their frequencies, which have been determined with a relative uncertainty of about 2×10^{-11}, were recommended by Bureau International des Poids et Mesures (BIPM) as a practical realization of meter and secondary representation of the second.

Here we present the frequency metrology of the $^{12}C_2H_2$ lines in the $\nu_1 + 3\nu_3$ band, which is located near 789 nm. These lines have also been extensively studied to derive spectroscopic parameters including line positions [18–20], line strengths [21,22], and collision-induced line shift and broadening coefficients [23–26]. The spectra were also used to investigate the ro-vibrational energy transfer mechanism [1,27–29]. In the energy levels presented recently by Chubb et al. [9], the rotational energies in the 1030^00^0 state, the upper state of the $\nu_1 + 3\nu_3$ band, were presented with a stated precision of 5×10^{-4} cm^{-1}.

Note that in the MARVEL analysis by Chubb et al. [9], the line positions from Ref. [21] were used but more accurate values from Ref. [30] have not been considered. In the study by Liu et al. [30], the centers of about 50 lines in the $\nu_1 + 3\nu_3$ band [30] were derived with a precision at the 10^{-5} cm^{-1} level from the fit of the Doppler-broadened spectrum recorded by cavity ring-down spectroscopy (CRDS). Nevertheless, the line center determined from a fit of the Doppler-broadened spectrum is often shifted by nearby lines which were not properly included in the fit, either from a weaker band or from contamination in the sample. The shift presents as a systematic uncertainty which cannot be eliminated by averaging. Such a problem can be solved by deriving the line positions from narrow Lamb dips instead of Doppler-broadened lines. The saturation spectrum of the P(11) line in this band has been recorded by Ma et al. [31] using noise-immune cavity-enhanced optical heterodyne molecular spectroscopy (NICE–OHMS), but its central frequency was not reported. Recently, we have demonstrated [32] the determination of the frequencies of a few CO lines near 1566 nm with a fractional accuracy of

* Corresponding author at: Hefei National Laboratory for Physical Sciences at Microscale, iChem center, University of Science and Technology of China, Hefei 230026, China.
E-mail address: smhu@ustc.edu.cn (S.-M. Hu).

https://doi.org/10.1016/j.jqsrt.2018.02.021
0022-4073/

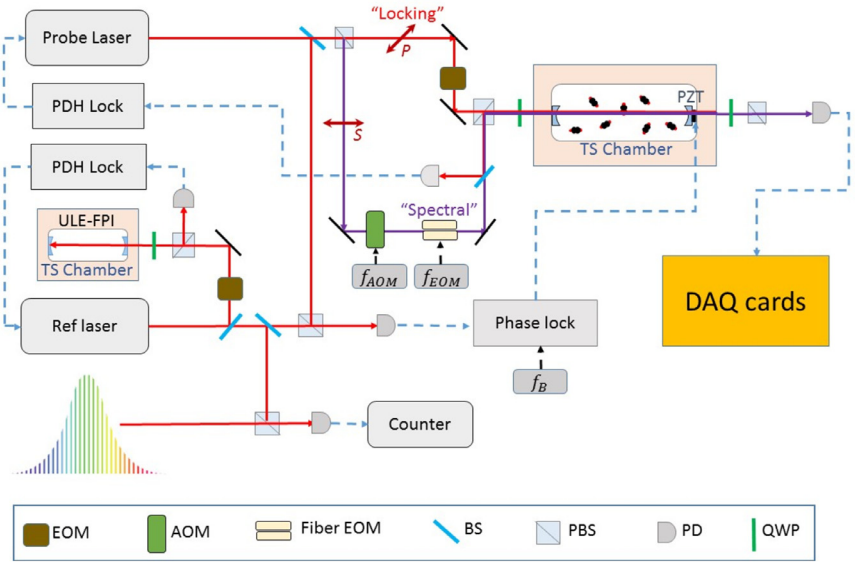

Fig. 1. Configuration of the experimental setup. One beam (red) from ECDL (external cavity diode laser) is used to lock the laser frequency to the cavity; another beam (purple) with a frequency shift of f_{AOM} +f_{EOM} is used for ring-down detecting. The cavity length is locked through the beat signal between ECDL and a reference laser. Abbreviations: AOM: acousto-optical modulator; BS: beam splitter; DAQ: data acquisition system; EOM: electro-optical modulator; PBS: polarized beam splitter; PD: photodiode detector; PZT: piezo actuator; QWP: quarter-wave plate. (For interpretation of the references to colour in this figure legend, the reader is referred to the web version of this article.)

2.6×10^{-12} using comb-locked cavity ring-down saturation spectroscopy [33]. Here, we extend the spectral region to 790 nm and present Lamb-dip measurements of 45 lines of $^{12}C_2H_2$ in the range of 12,612–12,714 cm^{-1}. The line positions were compared with previous Doppler-limited studies, and also the transitions derived from the energy levels given by Chubb et al. [9].

2. Experimental

The experimental setup is similar to the comb-locked cavity ring-down spectrometer described in Refs. [32,34]. The optical layout is shown in Fig. 1. The probe laser is an external cavity diode laser (ECDL, Toptica DL100) which is locked to a temperature-stabilized ring-down (RD) cavity by the Pound–Drever–Hall (PDH) method [35]. The RD cavity is composed of a pair of high-reflectivity (99.995%) mirrors setting apart with a distance of 45.9 cm, leading to a free spectral range (FSR) of 327 MHz, a finesse of 70,000 and a mode width of 4.6 kHz. The RD cavity is thermo-stabilized at 300 K with a fluctuation less than 2 mK in several hours [36]. A phase-lock circuit locks the cavity length through a piezo actuator (PZT) using the beat signal between the probe laser and a reference laser. The reference laser (Ti:Sapphire, Coherent MBR) is locked to a thermo-stabilized Fabry–Pérot interferometer (FPI) made of ultra-low-expansion (ULE) glass. An optical frequency comb operated at 780 nm is used to measure the frequency of the reference laser. The comb is synthesized by an Er:fiber oscillator (1.56 μm) with its repetition frequency (f_r) and carrier offset frequency (f_0) referenced to a GPS-disciplined rubidium clock (SRS FS725).

A separated beam from the probe laser, with its frequency shifted by an acousto-optical modulator (AOM) and an electro-optical modulator (EOM), is used for spectral probing. When the frequency shift is exactly an integral multiple of FSR, one of the 1st-order sidebands in the beam will be coupled into the RD cavity. The AOM also serves as an optical switch to produce the ring-down signal. A fitting program based on the Levenberg–Marquardt algorithm is applied to fit the curve to an exponential decay function. The sample absorption coefficient can be determined from:

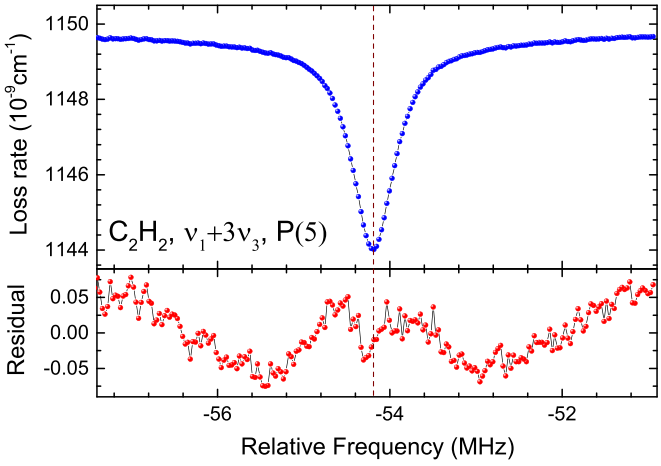

Fig. 2. Lamb-dip spectrum (40 scans average) of the P(5) line in the $\nu_1 + 3\nu_3$ band of $^{12}C_2H_2$ recorded at a sample pressure of 1.5 Pa. The lower panel shows the residuals of the fit using a Lorentzian function.

$$\alpha = \frac{1}{c\tau} - \frac{1}{c\tau_0} \quad (1)$$

where c is the speed of light, τ and τ_0 are the decay times of the cavity with and without sample, respectively. The loss rate of the empty cavity $(c\tau_0)^{-1}$ is 1×10^{-6} cm^{-1}. The spectral scan is accomplished by tuning the reference frequency f_B of the phase-lock loop:

$$\nu = f_{ref} + f_{AOM} + f_{EOM} + f_B \quad (2)$$

where f_{ref} is the frequency of the reference laser measured with the optical comb, and f_{AOM} and f_{EOM} are the radio frequencies driving the AOM and EOM, respectively.

3. Results and discussion

Fig. 2 shows the Lamb dip of the P(5) line in the $\nu_1 + 3\nu_3$ band of $^{12}C_2H_2$ recorded under a sample pressure of 1.5 Pa. The

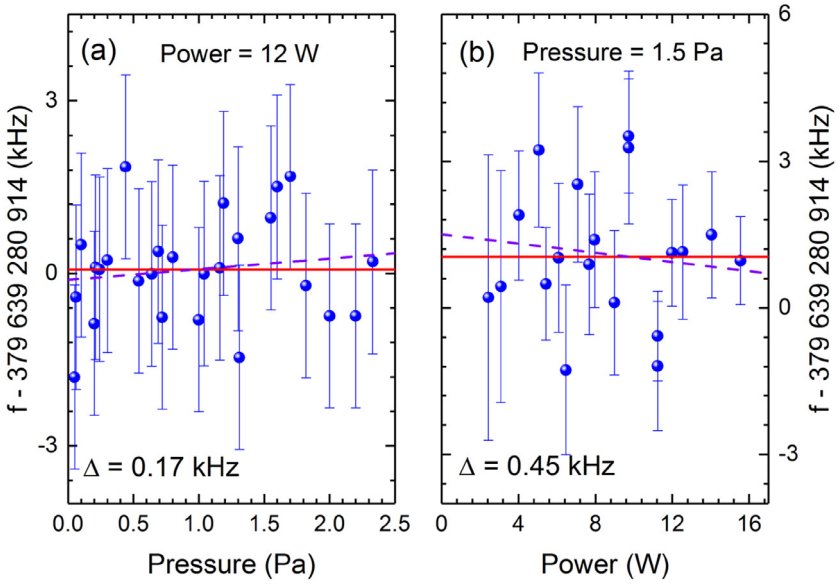

Fig. 3. Line positions of the P(5) line obtained at different sample pressures and intra-cavity laser powers. (a) Line positions from spectra with different sample pressures at a laser power of 12 W. (b) Line positions from spectra with different laser powers at a sample pressure of 1.5 Pa. The solid horizontal lines and the dashed lines show the weighted averaging and the linear fit of the date, respectively.

spectrum is an average of 40 scans, and over a span of 6.5 MHz. The P(5) line at 12663.403 cm^{-1} has a line intensity of 1.5×10^{-23} cm/molecule [21], the Einstein coefficients is 0.03 s^{-1}, and the saturation intensity [37] is 38 kW/cm^2. The inlet power coupled into the cavity was about 1 mW, which results in an intra-cavity power of about 12 W according to the formula given in Ref. [32]. It leads to a saturation parameter of about 0.1 at a laser beam waist radius of 0.5 mm. Since the main purpose of the present study is to determine precise line positions instead of the profile, each RD signal was fit with a pure exponential function for the sake of simplicity in spite of the non-exponential shape in the saturated regime. A Lorentzian function was used to fit the Lamb-dip spectrum, which yielded a width (half width at half maximum, HWHM) of about 300 kHz and a dip depth of 6×10^{-9} cm^{-1}. According to the residuals shown in Fig. 2, the amplitude of the fitting residual around peak center is about 1 % of the depth of the Lamb dip. Therefore, we estimate that the shift due to the asymmetry in the line profile, if any, should be below 3 kHz, about 1% of the half width of the Lamb dip.

A series of measurements were carried out to investigate the pressure shift and power shift under different experimental conditions. Fig. 3 shows the line positions of the P(5) line obtained at different pressures and different intra-cavity laser powers. Each data point was derived from a spectrum averaged from 100 to 200 scans. Using a linear fit of the data, we obtained a pressure-shift coefficient of 0.18 ± 0.26 kHz/Pa at a fixed power of 12 W and a power-shift coefficient of -0.05 ± 0.09 kHz/W at a pressure of 1.5 Pa. Note that the pressure-induced shift was reported to be -0.011 cm^{-1}/atm (-3.3kHz/Pa) in the Doppler regime [24], completely different from the value given here. Similar phenomena has been observed in previous studies [31,32]. Since we did not find obvious pressure shift and power shift under present experimental conditions, we finally used the simple average of the positions derived from different spectra. For other lines studied in this work, we took the sample pressure of 1.5 Pa and the intra-cavity laser power of 12 W, and gave an uncertainty of 0.17 kHz and 0.45 kHz for possible contributions from the pressure shift and the power shift, respectively.

The position of P(5) is determined to be 379 639 280 915.0 kHz and the uncertainty budget is presented in Table 1. By averaging the results derived from 4400 spectra recorded in 70 h in total, we obtained a statistical uncertainty of 0.5 kHz. As discussed above, an uncertainty of 3 kHz was assigned for the possible asymmetry in the line profile. The frequency comb used for calibration has an uncertainty of 0.8 kHz due to the long term stability of 2×10^{-12} from the Rb clock. The frequency shift due to the bias in the cavity locking servo is less than 0.1 kHz. The uncertainty in the driving frequencies of the AOM and EOM are negligible. Taking a root-square-mean velocity of 535 m/s of the $^{12}C_2H_2$ molecule at 300 K, the second-order Doppler shift is 0.6 kHz. The recoil shift cancels in saturation spectroscopy [38] therefore not included here. The overall uncertainty of the P(5) line position is 3.2 kHz, corresponding to a relative accuracy of 8×10^{-12}.

Table 1
Uncertainty budget of the P(5) line in the $\nu_1 + 3\nu_3$ band of $^{12}C_2H_2$ (in kHz).

Source	Frequency	Uncertainty	
		Type A	Type B
Statistical	379 639 280 914.4	0.5	
Frequency comb			0.8
Line profile asymmetry			3
Cavity locking servo			0.1
EOM frequency			0.001
AOM frequency			0.05
Pressure shift	0		0.17
Power shift	0		0.45
Second-order doppler	0.6		–
Total	379 639 280 915.0	3.2	

In total, 45 lines in the $\nu_1 + 3\nu_3$ band were measured and the maximum J value is 22. Their line positions are given in Table 2. The depths of the Lamb dips, observed at a sample pressure of 1.5 Pa and an intra-cavity laser power of about 12 W, are also given in the table. Typically the depth is about 4 % of the absorbance at the line center, agreeing well with the estimated saturation parameter. The depths exhibit a clear zigzag structure, indicating a dependence on the ortho-para symmetry of the levels. The differences from those obtained from the previous Doppler-broadened CRDS measurement [30] are also given in the table. Excluding the doppler-broadened lines perturbed by nearby water lines, we found an averaged shift of $8 \pm 3 \times 10^{-5}$$cm^{-1}$, which

Table 2
Positions of the lines in the $\nu_1+3\nu_3$ band of $^{12}C_2H_2$ (in cm^{-1}).

	ν, this work	D[a]	$\Delta\nu$[b] $\times 10^6$		ν, this work	D[a]	$\Delta\nu$[b] $\times 10^6$	$\Delta E''_{\nu_1+\nu_3}$[c]	δ[d] $\times 10^8$
P(1)	12 673.323 306 55(11)	1.6							
P(2)	12 670.919 290 93(11)	1.1		R(0)	12 677.979 111 34(12)	0.5		7.059 820 36(08)	5(18)
P(3)	12 668.464 589 07(11)	4.0	67	R(1)	12 680.230 826 58(11)	2.7	69	11.766 237 16(12)	35(19)
P(4)	12 665.959 248 56(11)	1.8	47	R(2)	12 682.431 707 52(11)	1.4	[e]106	16.472 458 62(13)	34(20)
P(5)	12 663.403 324 01(11)	5.8	105	R(3)	12 684.581 730 71(11)	4.5	105	21.178 406 70(13)	0(20)
P(6)	12 660.796 880 62(11)	2.3	88	R(4)	12 686.680 884 09(11)	2.3	90	25.884 003 59(11)	-12(20)
P(7)	12 658.140 043 09(11)	6.0	77	R(5)	12 688.729 214 03(11)	6.0	86	30.589 170 94(12)	0(20)
P(8)	12 655.432 966 24(11)	2.5	106	R(6)	12 690.726 796 77(11)	2.5	75	35.293 830 91(10)	-38(19)
P(9)	12 652.673 497 88(11)	6.0	110	R(7)	12 692.671 403 24(11)	6.7	104	39.997 905 19(11)	17(19)
P(10)	12 649.866 524 05(11)	2.6	59	R(8)	12 694.567 839 88(11)	2.5	86	44.701 315 93(14)	-11(21)
P(11)	12 647.008 684 33(11)	6.0	81	R(9)	12 696.412 669 19(11)	6.7	82	49.403 985 11(13)	-25(20)
P(12)	12 644.100 885 58(11)	2.3	86	R(10)	12 698.206 720 10(11)	2.7	[e]182	54.105 834 65(12)	-14(19)
P(13)	12 641.140 029 47(11)	4.0	[e]800	R(11)	12 699.946 816 22(11)	4.3	140	58.806 786 65(14)	-26(20)
P(14)	12 638.136 134 68(11)	1.9	12	R(12)	12 701.642 897 78(11)	2.2	72	63.506 763 18(14)	-43(21)
P(15)	12 635.079 452 73(11)	4.5	75	R(13)	12 703.285 139 33(11)	5.5	93	68.205 686 60(10)	-1(18)
P(16)	12 631.976 499 46(11)	1.7	45	R(14)	12 704.879 977 88(11)	2.0	74	72.903 478 43(09)	-2(18)
P(17)	12 628.827 591 13(11)	3.6	63	R(15)	12 706.427 652 34(11)	4.2	36	77.600 061 32(11)	-11(18)
P(18)	12 625.607 049 60(12)	0.6	94	R(16)	12 707.902 406 52(12)	0.7	57	82.295 357 31(10)	-39(20)
P(19)	12 622.463 226 00(12)	0.9	-12	R(17)	12 709.452 514 51(11)	1.7	62	86.989 288 47(09)	4(18)
	12 622.135 380 51(14)	0.4	138		12 709.124 668 97(15)	0.4	29		-1(22)
P(20)	12 619.055 766 08(12)	0.6	58	R(18)	12 710.737 543 14(12)	0.9	116	91.681 777 37(09)	-32(19)
P(21)	12 615.688 344 61(11)	1.7	73	R(19)	12 712.061 090 80(11)	2.3	100	96.372 746 06(09)	13(18)
P(22)	12 612.323 916 41(12)	0.5	124	R(20)	12 713.386 033 06(12)	0.7	[e]295	101.062 116 91(09)	-27(19)

[a] Depth of the Lamb dip observed at a sample pressure of 1.5 Pa and an intra-cavity laser power of 12 W, in 10^{-9} cm^{-1}.
[b] $\Delta\nu = \nu_{DB} - \nu_{tw}$, where ν_{tw} is determined from saturation spectroscopy (this work) and ν_{DB} is from the Doppler-broadened spectroscopy [30].
[c] $\Delta E'' = \nu'_{R(J)} - \nu'_{P(J+2)}$, ground state combination difference from Ref. [15], where ν' is the frequency of the transition in the $\nu_1+\nu_3$ band.
[d] The difference between the ground state combination difference from this work and that from Ref. [15], $\delta = \Delta E''_{\nu_1+3\nu_3} - \Delta E''_{\nu_1+\nu_3}$. The value given in the parenthesis is the combined uncertainty of both $\Delta E''$ values.
[e] The C_2H_2 line is close to a known water line. The Doppler-broadened C_2H_2 line center could be shifted.

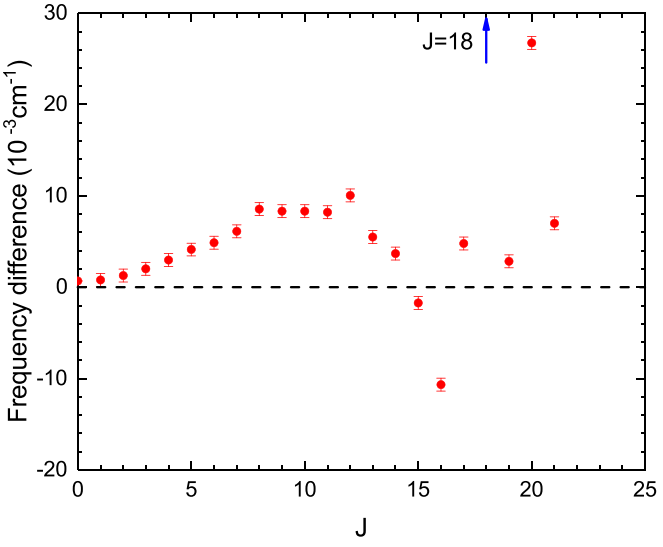

Fig. 4. Difference between the upper level energies given by Chubb et al. [9] and those from this work. The difference for the $J = 18$ level is over 0.1 cm^{-1} therefore not shown here.

is larger than the claimed uncertainty of 3×10^{-5}cm^{-1} given in Ref. [30]. A possible reason could be the long-term frequency drift of the Fabry–Pèrot interferometer used for calibration in previous study. We also calculated the ground state combination differences from the P and R transitions obtained in this work. They agree well with the combination differences derived from the lines in the $\nu_1+\nu_3$ band [15] which are also presented in Table 2.

Using ground state rotational level energies derived from the parameters given in Ref. [15], we determined the energies of the upper levels in the 1030^00^0 state. They were compared with the energies given by Chubb et al. [9] and the differences are depicted in Fig. 4. The error bars are the stated uncertainties given in Ref. [9] which are around 5×10^{-4} cm^{-1}. As shown in the figure, the deviation regularly increases for $J \le 8$, then oscillates after $J \ge 12$. Note that for the well-known $J = 18$ doublets [18,29,30], both transitions to the interacting levels were measured and their positions are given in Table 2. But only one energy level (13069.24864 cm^{-1}) around the position was given by Chubb et al., and the differences to both upper levels determined here are over 0.1 cm^{-1}. Excluding the $J = 18$ level, the maximum deviation reaches 0.027 cm^{-1} at $J = 20$. It is over 50 times of the uncertainty claimed in Ref. [9].

4. Conclusion

In conclusion, we recorded the saturation spectra of 45 lines in the $\nu_1+3\nu_3$ band of $^{12}C_2H_2$ using the comb-locked cavity ring-down spectroscopy. Although these lines are weaker than the $^{12}C_2H_2$ lines at 1.54 μm by two orders of magnitude, their frequencies were determined with an accuracy as good as 3.2 kHz (1.1×10^{-7} cm^{-1}), being comparable to that of the 1.54 μm acetylene frequency standards recommended by BIPM. These line positions can be used as accurate frequency grids in the spectral region of 786–793 nm.

Acknowledgments

This work was jointly supported by NSFC (nos. 91436209, 21427804, 21688102) and by CAS (no. XDB21020100).

References

[1] Orr BJ. Spectroscopy and energetics of the acetylene molecule: dynamical complexity alongside structural simplicity. Int Rev Phys Chem 2006;25:655–718.
[2] Silvestri F, Marrocchi A. Acetylene-based materials in organic photovoltaics. Int J Mol Sci 2010;11:1471–508.
[3] Travis AS. Unintended technology transfer: acetylene chemistry in the united states. Bull Hist Chem 2007;32:27–34.
[4] Orton GS, Aumann HH. The abundance of acetylene in the atmosphere of Jupiter. Icarus 1997;32:431–6.

[5] Rodgers SD, Charnley SB. Chemical differentiation in the region of massive star formation. Astrophys J 2001;546:324–9.
[6] Yu S, Drouin BJ, Pearson JC. Terahertz spectroscopy of the bending vibrations of acetylene $^{12}C_2H_2$. Astrophys J 2009;705:786–90.
[7] Amyay B, Fayt A, Herman M, Auwera JV. Vibration-rotation spectroscopic database on acetylene, $\tilde{X}^1\Sigma_g^+$ $^{12}C_2H_2$. J Phys Chem Ref Data 2016;45:023103.
[8] Lyulin OM, Perevalov VI. ASD-1000: High-resolution, high-temperature acetylene spectroscopic databank. J Quant Spectrosc Radiat Transfer 2017;201:94–103.
[9] Chubb KL, Joseph M, Franklin J, Choudhury N, Furtenbacher T, Császár AG, Gaspard G, Oguoko P, Kelly A, Yurchenko SN, Tennyson J, Sousa-Silva C. Marvel analysis of the measured high-resolution rovibrational spectra of C_2H_2. J Quant Spectrosc Radiat Transfer 2018;204:42–55.
[10] Hong FL, Onae A, Jiang J, Guo RX, Inaba H, Minoshima K, Schibli TR, Matsumoto H, Nakagawa K. Absolute frequency measurement of an acetylene-stabilized laser at 1542 nm. Opt Lett 2003;28:2324–6.
[11] de Labachelerie M, Nakagawa K, Ohtsu M. Ultranarrow $^{13}C_2H_2$ saturated-absorption lines at 1.5 µm. Opt Lett 1994;19:840–2.
[12] Czajkowski A, Madej AA, Dube P. Development and study of a 1.5 µm optical frequency standard referenced to the p(16) saturated absorption line in the $\nu_1+\nu_3$ overtone band of $^{13}C_2H_2$. Opt Commun 2004;234:259–68.
[13] Edwards CS, Barwood GP, Margolis HS, Gill P, Rowley WRC. High-precision frequency measurements of the $\nu_1+\nu_3$ combination band of $^{12}C_2H_2$ in the 1.5 µm region. J Mol Spectrosc 2005;234:143–8.
[14] Edwards CS, Margolis HS, Barwood GP, Lea SN, Gill P, Rowley WRC. High-accuracy frequency atlas of $^{13}C_2H_2$ in the 1.5 µm region. Appl Phys B 2005;80:977–83.
[15] Madej AA, Alcock AJ, Czajkowski A, Bernard JE, Chepurov S. Accurate absolute reference frequencies from 1511 to 1545 nm of the $\nu_1+\nu_3$ band of $^{12}C_2H_2$ determined with laser frequency comb interval measurements. J Opt Soc Am B 2006;23:2200–8.
[16] Madej AA, Bernard JE, Alcock AJ, Czajkowski A, Chepurov S. Accurate absolute frequencies of the $\nu_1+\nu_3$ band of $^{13}C_2H_2$ determined using an infrared mode-locked Cr: YAG laser frequency comb. J Opt Soc Am B 2006;23:741–9.
[17] Gatti D, Gotti R, Gambetta A, Belmonte M, Galzerano G, Laporta P, Marangoni M. Comb-locked Lamb-dip spectrometer. Sci Rep 2016;6:27183.
[18] Smith BC, Winn JS. The overtone dynamics of acetylene above 10,000 cm^{-1}. J Chem Phys 1991;94:4120–30.
[19] Zhan XW, Halonen L. High-resolution photoacoustic study of the $\nu_1+3\nu_3$ band system of acetylene with a titanium-sapphire ring laser. J Mol Spectrosc 1993;160:464–70.
[20] Hurtmans D, Kassi S, Depiesse C, Herman M. Assignment of a perturbation in the FT-ICLAS spectrum of $^{12}C_2H_2$ around 12 709.5 cm^{-1}. Mol Phys 2002;100:3507–11.
[21] Herregodts F, Kerrinckx E, Huet TR, Auwera JV. Absolute line intensities in the $\nu_1+3\nu_3$ band of $^{12}C_2H_2$ by laser photoacoustic spectroscopy and fourier transform spectroscopy. Mol Phys 2003;101:3427–38.
[22] Macko P, Herman M. Absolute line intensity with FT-ICLAS: $^{12}C_2H_2$ near 12,800 cm^{-1}. Chem Phys Lett 2006;417:471–4.
[23] Lucchesini A, DeRosa M, Pelliccia D, Ciucci A, Gabbanini C, Gozzini S. Diode laser spectroscopy of overtone bands of acetylene. Appl Phys B 1996;63:277–82.
[24] Herregodts F, Hepp M, Hurtmans D, Auwera JV, Herman M. Laser spectroscopy of the $\nu_1+3\nu_3$ absorption band in $^{12}C_2H_2$. II. self-collisional lineshift measurements. J Chem Phys 1999;111:7961.
[25] Herregodts F, Hurtmans D, Auwera JV, Herman M. Ar-induced pressure effects in the $\nu_1+3\nu_3$ absorption band in $^{12}C_2H_2$. Chem Phys Lett 2000;316:460–4.
[26] Valipour H, Zimmermann D. Investigation of J dependence of line shift, line broadening, and line narrowing coefficients in the $\nu_1+3\nu_3$ absorption band of acetylene. J Chem Phys 2001;114:3535.
[27] Metsälä M, Yang S, Vaittinen O, Halonen L. Laser-induced dispersed vibration-rotation fluorescence of acetylene: spectra of ortho and para forms and partial trapping of vibrational energy. J Chem Phys 2001;117:8686–93.
[28] Payne MA, Milce AP, Frost MJ, Orr BJ. Rovibrational energy transfer in the $4\nu_{CH}$ manifold of acetylene, viewed by IR-UV double resonance spectroscopy. 1. foundation studies at low *j*. J Phys Chem A 2003;107:10759–70.
[29] Payne MA, Milce AP, Frost MJ, Orr BJ. Rovibrational energy transfer in the $4\nu_{CH}$ manifold of acetylene viewed by IR-UV double resonance spectroscopy. 2. perturbed states with $J=17$ and 18. J Phys Chem B 2005;109:8332–43.
[30] Liu AW, Li XF, Wang J, Lu Y, Cheng CF, Sun YR, Hu SM. H_2O line positions in the 784–795 nm region with 10^{-9} accuracy. J Chem Phys 2013;138:014312.
[31] Ma LS, Ye J, Dube P, Hall JL. Ultrasensitive frequency-modulation spectroscopy enhanced by a high-finesse optical cavity: theory and application to overtone transitions of C_2H_2 and C_2HD. J Opt Soc Am B 1999;16:2255–68.
[32] Wang J, Sun YR, Tao LG, Liu AW, Hu SM. Communication: molecular near-infrared transitions determined with sub-khz accuracy. J Chem Phys 2017;147:091103.
[33] Wang J, Sun YR, Tao LG, Liu AW, Hua TP, Meng F, Hu SM. Comb-locked cavity ring-down saturation spectroscopy. Rev Sci Instrum 2017;88:043108.
[34] Chen J, Hua TP, Tao LG, Sun YR, Liu AW, Hu SM. Absolute frequencies of water lines near 790 nm with 10^{-11} accuracy. J Quant Spectrosc Radiat Transfer 2018;205:91–5.
[35] Drever RWP, Hall JL, Kowalski FV, Hough J, Ford GM, Munley AJ, Ward H. Laser phase and frequency stabilization using an optical-resonator. Appl Phys B 1983;31:97–105.
[36] Cheng CF, Wang J, Sun YR, Tan Y, Kang P, Hu SM. Doppler broadening thermometry based on cavity ring-down spectroscopy. Metrologia 2015;52:S385–93.
[37] Giusfredi G, Bartalini S, Borri S, Cancio P, Galli I, Mazzotti D, De Natale P. Saturated-absorption cavity ring-down spectroscopy. Phys Rev Lett 2010;104:110801.
[38] Hall JL, Borde CJ, Uehara K. Direct optical resolution of recoil effect using saturated absorption spectroscopy. Phys Rev Lett 1976;37:1339–42.